Wave-induced steady currents by submerged canopy-oscillatory flow interaction

A. Cáceres-Euse[1,2], A. Orfila[3], M. Maza[4], G. Besio[2]

[1]Mediterranean Institute of Oceanography, MIO, Université de Toulon, 83041 Toulon, Cedex 9, France
[2]University of Genova, Department of Civil, Chemical and Environmental Engineering (DICCA), MeteOcean Group, Italy
[3]Mediterranean Institute for Advanced Studies, IMEDEA (CSIC-UIB), 07190 Esporles, Spain
[4]IH Cantabria - Instituto de Hidráulica Ambiental de la Universidad de Cantabria, 39011, Santander, Spain

Key Points:

- A new analytical model is presented for wave-induced steady current by performing a dimensional analysis
- The model reveals that the wave decay (pressure gradient) contributes to wave-induced steady current
- The steady current is driven by the pressure gradient, wave-steady current interaction drag, and wave and Reynolds stress gradient terms

Corresponding author: A. Cáceres-Euse, acacere@unal.edu.co

Abstract

A new analytical model is presented in order to better understand the depth-dependent wave-induced steady current caused by submerged aquatic canopy-oscillatory flow interaction. The analytical model takes into account the wave and canopy properties. The model is developed by determining the dominant terms in the momentum equation by means of dimensional analysis and satisfying the mass conservation. The dimensional analysis reveals that the pressure gradient (due to wave decay) is of the same order of magnitude as the drag force, wave stress and Reynolds stress terms. In addition, the balance between the pressure gradient and mass conservation induces a seaward current above the canopy, and the presence of the pressure gradient in the momentum equation contributes to intensify the skimming flow at the top of the canopy. Finally, given that the model follows a polynomial function it can be easily implemented in large scale models such as phase average models.

Plain Language Summary

Submerged aquatic canopies are present worldwide modifying the surrounding coastal flow (such as mean onshore currents and wave orbital velocities) and dissipating incoming wave heights. Nonetheless, the mechanism and dominant terms in generating wave-induced steady currents under submerged canopies-wave interaction is not well understood. By applying dimensional analysis to 2-D momentum equation along with parametrizations to the wave stress gradient and pressure gradient (wave decay) terms, we observed that the wave-induced steady current can be split in three regions: above the canopy top where the steady current goes seaward, at the canopy top where the current goes shoreward, and inside the canopy where the current is very weak compared to the previous regions (less than 10% the above-canopy orbital velocity). This simplified model can give us insights about the residence time, horizontal nutrient and sediment transport processes in coastal canopies, and can be easy to implement in large scale coastal models.

1 Introduction

Aquatic canopies cover large areas in shallow coastal waters are among the most biologically diverse and productive components of coastal systems. Canopy meadows are net sink for atmospheric CO2 (Duarte et al., 2010) and provide a wide range of ecosystem services (Chen et al., 2019). From the hydrodynamic perspective, aquatic canopies are an efficient system to dissipate energy from waves and surges by increasing damping thus protecting and preventing coastal shores from erosion (Maxwell et al., 2017; Foster-Martinez et al., 2018). These canopies are exposed to long waves (shallow water wave conditions) where the oscillatory flow dominates hydrodynamics and turbulent features (Abdolahpour et al., 2020).

The vegetation-oscillatory flow interaction begins with the dissipation of the incoming wave due to the work done by the canopy elements (Dalrymple et al., 1984; Kobayashi et al., 1993; Losada et al., 2016; Lei & Nepf, 2019), the wave orbital velocity attenuation inside the canopy due to the drag resistance by the stems against the flow (Lowe et al., 2005; Abdolahpour et al., 2016), and the generation of turbulence within the stems (wake scale) (Nepf, 2012; Tanino & Nepf, 2008; Zhang et al., 2018).

The reduction in the wave orbital velocity magnitude by the stems generates a strong discontinuity in the horizontal orbital velocity component (a shear layer) at the top of the submerged canopy enhancing the vertical mixing across the top of the canopy by a Kelvin-Helmholtz-type vortex instability (KH). The KH can occur if the wave excursion is much larger than the canopy drag length scale and the inertia of the flow overcomes the viscosity (Abdolahpour et al., 2016; Ghisalberti & Nepf, 2002; Ghisalberti & Schlosser, 2013). This shear layer causes the discrepancy in the Stokes drift velocity at the top of

the canopy compared with the non-dissipative linear wave theory (Jacobsen, 2016). Recently, Abdolahpour et al. (2020) highlighted that the vertical mixing due to the shear layer and the advective transport by a steady current shoreward, have serious implications on the residence time (i.e., the time scale of water parcels retained within the canopy), which in turn have biogeochemical implications.

To date, few studies have been developed regarding the steady current shoreward in aquatic canopy-wave interaction (wave-induced steady current). Experimental and field studies reported that the presence of a shear layer near the top of the coastal canopy induces a streaming flow (analogous to streaming flows in wave boundary layers) as function of the drag forces creating a steady current shoreward (Luhar et al., 2010, 2013). Luhar et al. (2010) showed both analytically and experimentally that the work done by the stems on the flow produces a nonzero time-averaged wave stress at the top of the canopy, estimating a depth-integrated steady current. This nonzero wave stress hypothesis was later validated using a Reynolds Averaged Navier-Stokes-Volume of Fluid numerical model (RANS-VOF) in Chen et al. (2019). Nonetheless, recently, Abdolahpour et al. (2017, 2020) demonstrated that the steady current shoreward has a strong gradient along the water depth for submerged canopies with a maximum value at the top of the canopy. This maximum value not only depends on the drag forces but also on the wave orbital excursion (wave parameter). In addition, van Rooijen et al. (2020), using a shallow water equation model (SWASH), determined that along with the wave stress and the drag force, the Reynolds stress tensor plays a relevant role in the steady current generation.

From this background, it is clear that the role of the dominant terms in the momentum equation, involved in the wave-induced steady current, is not yet well understood. A first step towards this goal is the development of an analytical model able to represent the main features of the steady current profile along the water column, which could be easily applied in large scale coastal models (particularly *phase averaged models*).

To take a step forward in our understand of the wave induced steady current by canopy vegetation-wave interaction, the aim of this work is to answer two main questions: 1) what are the dominant terms in the momentum equation involved in the wave-induced steady current under aquatic canopies-wave interaction? and 2) is it possible to develop a simplified analytical model capable to estimate the depth-dependent wave-induced steady current as a function of the wave parameters and canopy properties?.

In this work, an analytical model for the long wave induced steady currents is developed and compared against experimental data for rigid canopies, and against the numerical simulations from a RANS-VOF model for flexible canopies. The paper is structured as follows: in Section 2 the analytical model is obtained by scaling the 2D Navier-Stokes equations, and parameterizing the wave and Reynolds stress terms. In section 3 the analytical model is validated against experimental data for rigid canopies and numerical RANS data for flexible elements. In addition, a discussion and general overview on wave-induced steady current is presented. Finally, the conclusions and future work are highlighted in section 4.

2 Development of the analytical model

2.1 Scaling the momentum equation

In this section, a 1D model for wave-induced steady currents shoreward is going to be presented. Following Cáceres-Euse et al. (2020), the model assumptions are summarized as:

1. the cross-stream direction is negligible compared to the stream-wise (wave propagation axis),

2. the seagrass-oscillatory flow environment can be assumed horizontal and parallel, and
3. the hydrostatic approximation is valid.

Under these hypothesis, the 2D momentum and mass conservation equations for the horizontal and vertical velocities and for the pressure are:

$$\frac{\partial u}{\partial t} + \frac{\partial u^2}{\partial x} + \frac{\partial wu}{\partial z} = -\frac{1}{\rho}\frac{\partial p}{\partial x} + \nu\left(\frac{\partial^2 u}{\partial x^2} + \frac{\partial^2 u}{\partial z^2}\right) + F_D, \tag{1}$$

$$\frac{\partial p}{\partial z} = -\rho g, \tag{2}$$

$$\frac{\partial u}{\partial x} = -\frac{\partial w}{\partial z}, \tag{3}$$

where ν and g are the kinematic fluid viscosity and the gravitational acceleration, respectively, F_D is the canopy resistance and ρ the density of seawater.

To determine the dominant terms for the wave-induced steady currents in the momentum equation, a scaling analysis is performed to equation (1). The reference variables for the scaling are, the wavelength, λ; the local water depth, h; a characteristic time scale of several wave periods, $\beta = \alpha T$ (with $\alpha >> 1$); the characteristic wave-induced horizontal steady current, $\hat{U}$; and the characteristic vertical velocity, $\hat{W}$. Accordingly, the following non-dimensional variables are defined:

$$u^* = \frac{u}{\hat{U}}, \quad w^* = \frac{w}{\hat{W}}, \quad p^* = \frac{p}{\rho g h}, \quad x^* = \frac{x}{\lambda}, \quad z^* = \frac{z}{h}, \quad t^* = \frac{t}{\beta}. \tag{4}$$

From the mass conservation equation (3) it follows that: $\frac{\hat{U}}{\lambda} \sim \frac{\hat{W}}{h}$, and thus, the characteristic vertical velocity can be defined as $\hat{W} \sim \hat{U}h/\lambda$ and the momentum equation (1) reads:

$$\frac{\hat{U}}{\beta}\frac{\partial u^*}{\partial t^*} + \frac{\hat{U}^2}{\lambda}\frac{\partial u^{*^2}}{\partial x^*} + \frac{\hat{U}^2}{\lambda}\frac{\partial w^* u^*}{\partial z^*} = -\frac{gh}{\lambda}\frac{\partial p^*}{\partial x^*} + \nu\left(\frac{\hat{U}}{\lambda^2}\frac{\partial^2 u^*}{\partial x^{*^2}} + \frac{\hat{U}}{h^2}\frac{\partial^2 u^*}{\partial z^{*^2}}\right) + F_D^*. \tag{5}$$

At this point we remark that $\lambda >> h$ since we are dealing with the shallow water wave regime. The last term in equation (5) represents the canopy resistance and will be analysed in detail later. From the above, $O(\beta) \sim 10^1$ to 10^2, $O(\lambda) \sim 10^1$ to 10^2, $O(h) \sim 10^0$, and $O(\hat{U}) \sim 10^{-1}$ to 10^0; thus, $O(\hat{U}/\beta) \sim O(\hat{U}/\lambda^2) \sim O(\hat{U}/h^2) << 1$ and the momentum equation (5), where the gradients are non-dimensional, reduces to:

$$\frac{\hat{U}^2}{\lambda}\frac{\partial u^{*^2}}{\partial x^*} + \frac{\hat{U}^2}{\lambda}\frac{\partial w^* u^*}{\partial z^*} = -\frac{gh}{\lambda}\frac{\partial p^*}{\partial x^*} + F_D^*. \tag{6}$$

Owing to the advective terms on the left hand side of equation (6) have the same order of magnitude, they can be grouped as:

$$\frac{\hat{U}^2}{\lambda}\frac{\partial u^{*^2}}{\partial x^*} + \frac{\hat{U}^2}{\lambda}\frac{\partial w^* u^*}{\partial z^*} \approx \Gamma\frac{\hat{U}^2}{\lambda}\frac{\partial w^* u^*}{\partial z^*}, \tag{7}$$

where $\Gamma = O(1)$ and consequently the momentum equation is:

$$\frac{\hat{U}^2}{\lambda}\frac{\partial w^* u^*}{\partial z^*} = -\frac{gh}{\lambda}\frac{\partial p^*}{\partial x^*} + F_D^*, \tag{8}$$

or in dimensional variables as,

$$\frac{\partial wu}{\partial z} = -\frac{1}{\rho}\frac{\partial p}{\partial x} + F_D. \tag{9}$$

The drag and inertial forces included in the canopy resistance F_D can be expressed by the Morrison equation (Dalrymple et al., 1984), as

$$F_D = \frac{1}{2} C_d A_v u \mid u \mid + A_v a_v C_M \frac{\partial u}{\partial t}, \tag{10}$$

where a_v is the diameter of the stem, $A_v = a_v N_v$ is the frontal canopy area per unit volume with N_v the number of canopy elements per unit area and C_d and C_M the drag and inertial coefficients respectively. The nondimensial form of equation (10) is:

$$F_D^* = \frac{1}{2} C_d A_v \hat{U}^2 u^* \mid u^* \mid + C_M A_v a_v \frac{\hat{U}}{\beta} \frac{\partial u^*}{\partial t^*}, \tag{11}$$

with $\hat{U}^2 u^* \mid u^* \mid >> \hat{U}/\beta(\partial u^*/\partial t^*)$ since $C_d \sim C_M$ (see for instance Lowe et al. (2005); Etminan et al. (2019)) and the dimensional momentum equation (9) ends,

$$\frac{\partial wu}{\partial z} = -\frac{1}{\rho}\frac{\partial p}{\partial x} + F_D, \qquad F_D = \frac{1}{2} C_d A_v u \mid u \mid . \tag{12}$$

Equation (12) represents the dominant terms in the momentum equation involved in the steady flow generated by submerged canopies in long wave conditions. Note that the pressure gradient is of the same order of magnitude as the vertical component of the advection (as well as of the drag force) contradicting previous studies that neglected this contribution given its unclear role on the generation of the wave-induced steady currents (Luhar et al., 2010, 2013; van Rooijen et al., 2020).

2.2 Time averaging and analytical solution

In this section, a time averaging over several wave periods is performed to equation (12) to determine the magnitude of the wave-induced steady currents. To calculate the wave-induced steady currents we average equation (12) over several wave periods. The horizontal and vertical velocities $\mathbf{u} = (u, w)$ are decomposed as,

$$\mathbf{u}(z,t) = \mathbf{u}_m(z,t) + \mathbf{u}'(z,t), \qquad \mathbf{u}_m(z,t) = \overline{\mathbf{u}}(z,t) + \tilde{\mathbf{u}}(z,t), \tag{13}$$

where $\mathbf{u}_m$ are the mean velocity components (waves plus steady currents), $\overline{\mathbf{u}}$ the time-independent mean velocity components, $\tilde{\mathbf{u}}$ the wave orbital velocity components and $\mathbf{u}'$ the turbulent velocity components. Recall that by definition:

$$\overline{\mathbf{u}} = \frac{1}{\beta}\int_t^{t+\beta} \mathbf{u}\,\mathrm{dt} \quad \text{and} \qquad \overline{\tilde{\mathbf{u}}} = \overline{\mathbf{u}'} = 0. \tag{14}$$

Replacing equation (13) into equation (12), applying the time averaging equation (14), and stating that waves and turbulence coexist but do not correlate between each other (Bricker & Monismith, 2007), results in $\overline{w_m u'} = \overline{w' u_m} = 0$. Additionally, given that $\overline{w} << \overline{u}$, one obtains $\overline{w}\ \overline{u} \approx 0$ and, through equation (14), $\overline{\tilde{w}\tilde{u}} = \overline{\tilde{w}}\,\overline{\tilde{u}} = 0$. Thus, the time averaged left hand side of equation (12) can be expressed as:

$$\frac{\partial \overline{wu}}{\partial z} = \frac{\partial \overline{\tilde{w}\tilde{u}}}{\partial z} + \frac{\partial \overline{w'u'}}{\partial z}, \tag{15}$$

where $\overline{\tilde{w}\tilde{u}}$ is the time-averaged wave stress and $\overline{w'u'}$ the time-averaged Reynolds stress.

Now, the drag force due to the canopy elements is function of the mean flow (wave and steady currents) (Finnigan, 2000; Nepf, 2012; Luhar et al., 2013), so the turbulent fluctuations can be neglected and the averaging to F_D in equation(12) can be defined as:

$$\overline{F_D} = \tfrac{1}{2} C_d A_v \overline{(\overline{u} + \tilde{u}) \mid \overline{u} + \tilde{u} \mid}. \tag{16}$$

To simplify Eq.(16), by definition,

$$\mid \overline{u}+\tilde{u} \mid \leq \mid \overline{u} \mid + \mid \tilde{u} \mid \quad \Rightarrow \quad (\overline{u}+\tilde{u}) \mid \overline{u}+\tilde{u} \mid \leq (\overline{u}+\tilde{u})(\mid \overline{u} \mid + \mid \tilde{u} \mid), \tag{17}$$

and applying the time averaging $\overline{\tilde{u} \mid \overline{u} \mid} = \overline{\tilde{u} \mid \tilde{u} \mid} = 0$, so the time-averaged momentum equation reduces to

$$\frac{\partial \overline{\tilde{w}\tilde{u}}}{\partial z} + \frac{\partial \overline{w'u'}}{\partial z} = -\frac{1}{\rho}\frac{\partial \overline{p}}{\partial x} + \frac{1}{2}C_d A_v \left(\overline{\overline{u} \mid \overline{u} \mid} + \overline{\overline{u} \mid \tilde{u} \mid} \right), \tag{18}$$

where $\overline{\overline{u} \mid \overline{u} \mid} = \overline{u} \mid \overline{u} \mid \sim O(\overline{u}^2)$ is negligible compared to the wave-steady current interaction term $\overline{\overline{u} \mid \tilde{u} \mid} \sim O(\overline{u}U_\infty)$. U_∞ is the horizontal wave orbital velocity.

The first term on the right hand side of equation (18) is formulated based on its maximum value, given its relevant role at the wavelength scale λ,

$$\frac{\partial \overline{p}}{\partial x} = \rho g \frac{\partial a}{\partial x}, \tag{19}$$

where a is the wave amplitude and can be expressed as a function of x (Dalrymple et al., 1984; Losada et al., 2016; Luhar et al., 2017):

$$a(x) = \frac{a_0}{1+\xi\, x}, \tag{20}$$

here ξ is a wave decay parameter (Dalrymple et al., 1984), and C_d is estimated based on Maza et al. (2013). Thus, the pressure gradient can be approximated within the meadow by using the effective vegetation length scale L_e as:

$$\frac{\partial \overline{p}}{\partial x} \approx -\frac{\rho g \xi a_0}{(1+\xi L_e)^2}, \tag{21}$$

being $L_e = (V - V_m)/A_v$, V a control volume, and V_m the volume of vegetation inside the control volume (Mazda et al., 1997). Thus, equation (18) can be finally stated as:

$$\frac{\partial \overline{\tilde{w}\tilde{u}}}{\partial z} + \frac{\partial \overline{w'u'}}{\partial z} = \frac{g\xi a_0}{(1+\xi L_e)^2} + \frac{1}{2}C_d A_v \overline{\overline{u} \mid \tilde{u} \mid}, \tag{22}$$

which is the time-averaged momentum equation dealing with the dominant terms involved in the wave-induced steady current released by aquatic canopy-oscillatory flow environments. This analytically developed equation, is similar to the numerical one presented by van Rooijen et al. (2020), but including the pressure gradient, the Reynolds stress, and the wave-steady current drag force effects. In the next, additional simplifications will be performed in order to find an analytical solution.

2.3 Analytical solution and parameterization

The Reynolds stress is (Rodi, 1993):

$$\overline{w'u'} = -\nu_t \frac{\partial \overline{u}}{\partial z}, \tag{23}$$

where ν_t is the eddy viscosity. Regarding the wave stress term, numerical experiments demonstrated a maximum value at the top of the canopy and zero elsewhere (Chen et al., 2019; van Rooijen et al., 2020). Thus, wave stress gradients at the top of the canopy, z=h_v, and Reynolds stress can be respectively simplified as:

$$\left(\frac{\partial \overline{\tilde{w}\tilde{u}}}{\partial z} \right)_{z=h_v} \approx \frac{\overline{\tilde{w}\tilde{u}}}{\delta} \approx \frac{\overline{\tilde{w}\tilde{u}}}{0.2A_w}, \qquad \frac{\partial \overline{w'u'}}{\partial z} = -\nu_t \frac{\partial^2 \overline{u}}{\partial z^2}, \tag{24}$$

where $\delta \approx 0.2A_w$ being A_w the horizontal wave orbital excursion and δ is the shear layer thickness (Cáceres-Euse et al., 2020). $A_w = U_\infty T/(2\pi)$ and U_∞ comes from the linear wave theory. The definition for ν_t is presented in the appendix section. Additionally, applying a skin friction formulation on a rough surface leads (Lowe et al., 2005; Jensen et al., 1989; Infantes et al., 2012; Foster-Martinez et al., 2018):

$$\frac{\overline{\tilde{w}\tilde{u}}}{\delta} \approx -\frac{f_w U_{\infty,rms}^2}{2\delta} \approx -\frac{f_w U_{\infty,rms}^2}{0.4A_w}, \tag{25}$$

where $U_{\infty,rms}$ is the root mean square of the horizontal wave orbital velocity far from the canopy effect and f_w the friction factor coefficient (Nielsen, 1992) see appendix). Replacing equation (24) into equation (22) results in:

$$\frac{\partial^2 \overline{u}}{\partial z^2} = \frac{1}{\nu_t}\left(-\frac{g a_0 \xi}{(1+\xi L_e)^2} + \left(\frac{\partial \overline{\tilde{w}\tilde{u}}}{\partial z}\right)_{z=h_v} - \frac{1}{2}C_d A_v \overline{\overline{u} \mid \tilde{u} \mid}\right). \tag{26}$$

Integrating vertically twice equation (26), and assuming that the wave-steady current interaction term can be simplified as $\overline{u} << \overline{\mid \tilde{u} \mid}$ (always below the top of the canopy), leads to $\overline{\overline{u} \mid \tilde{u} \mid} \approx U_c \overline{\mid \tilde{u} \mid}$ and $\overline{\mid \tilde{u} \mid} \leq U_h^{rms}$ where U_h^{rms} is the root mean square of the horizontal wave orbital velocity inside the canopy and U_c the steady current at the bottom. Additionally, $U_h^{rms} = \phi U_{\infty,rms}$ with $\phi < 1$ is the attenuation parameter (Lowe et al., 2005). The time averaged momentum equation (equation 26) can be finally written as:

$$\overline{u(z)} = \frac{z^2}{2\nu_t}\left(-\frac{g a_0 \xi}{(1+\xi L_e)^2} + \left(\frac{\partial \overline{\tilde{w}\tilde{u}}}{\partial z}\right)_{z=h_v} - \frac{1}{2}C_d A_v \phi U_c U_{\infty,rms}\right) + C_1 z + C_2, \tag{27}$$

with C_1 and C_2 integration constants and with $\overline{u(z)}$ satisfying the mass conservation:

$$\int_0^h \overline{u(z)} dz \approx 0. \tag{28}$$

Finally, applying the boundary condition at the bottom, *i.e.* $\overline{u(0)} = U_c$ we can write:

$$\overline{u(z)} = \left(\frac{3z^2 - 2zh}{6\nu_t}\right)\left(\frac{-g a_0 \xi}{(1+\xi L_e)^2} + f(z)\left(\frac{\overline{\tilde{w}\tilde{u}}}{0.2A_w}\right) - \frac{\epsilon}{2}C_d A_v \phi U_c U_{\infty,rms}\right) + U_c\left(1 - \frac{2z}{h}\right), \tag{29}$$

where $\epsilon = 1$ for $z \leq h_v$ and $\epsilon = 0$ for $z > h_v$, and,

$$f(z) = \begin{cases} 1 - \frac{1}{\delta} \mid h_v - z \mid, & z \in [h_v - \delta, h_v + \delta] \\ 0, & z \leq h_v - \delta \wedge z \geq h_v + \delta, \end{cases} \tag{30}$$

a delta function included to activate or deactivate the effect of the wave stress at the top of the canopy. Finally, the steady current at the bottom can be estimated assuming that drag coefficients for waves and current are comparable (Luhar et al., 2010), so that,

$$U_c = \sqrt{\frac{4}{3\pi}\frac{k}{\sigma}U_b^3}, \qquad U_b = \frac{3}{4}\frac{a^2 \sigma k}{sinh^2(kh)}, \tag{31}$$

where k, and σ are the wavenumber and angular frequency, and U_b the steady current in absence of canopy (Longuet-Higgins, 1953).

3 Validation and discussion of the analytical model

The vertical profile for steady current obtained with the analytical model is tested in this section for rigid vegetation using experimental data from van Rooijen et al. (2020)

Table 1. Experimental and numerical parameters. U_r the Ursell, Re Reynolds and KC Keulegan-Carpenter numbers.

	Van Rooijen et al. 2020				
ID	$H(m)$	$T(s)$	Re	KC	Ur
$R1$	0.14	2	1043	51	4.19
$R2$	0.10	3	1009	74	7.86
$R3$	0.21	3	1845	135	16.51
$R4$	0.20	4	1722	169	29.45
$R5$	0.09	5	1182	144	21.22
$R6$	0.21	5	1887	230	49.42
	Maza et al. 2013				
ID	$H(m)$	$T(s)$	$N(m^{-2})$	$h(m)$	Ur
$CM1$	0.44	3.5	180	2.4	6.91
$CM2$	0.49	4	360	1.8	20.26

and for flexible vegetation with numerical experiments from Maza et al. (2013). van Rooijen et al. (2020) performed experiments considering a rigid canopy under 6 different wave conditions. The tests were done in a 35 m long, 1.2 m deep, and 1.2 m wide wave flume. A Nortek Vectrino ADV measuring at 25Hz was placed at the midpoint of the canopy. The canopy was constructed as an staggered dowels array of 6.4 mm diameter, 30 cm high, approximately 3100 units per m^2 density, and 2.5 m long. Water depth was equal to 75 cm, wave heights ranged from 9 to 21 cm and wave periods from 2 to 5 s (see Table 1).

Regarding the numerical data for a flexible canopy, Maza et al. (2013) performed numerical simulations using a RANS-VOF model, including the stem flexibility and the relative displacement between the stems and the surrounding oscillatory flow. Two canopy density values were tested, 180 units per m^2 and 360 units per m^2. The stems were 55cm high (including their base), 1mm thick and 1cm width, and the material used to built them had a Young's modulus equal to 2.9 GPa. Wave height, water depth and wave period were defined according to Table 1.

3.1 Rigid canopy

Figure 1 displays the comparison of the normalized steady current of the experimental data and the analytical model for rigid canopies. The 95% confidence interval of the experimental data, estimated by using the interquartile and bootstraping methods, is also shown in the figure. Results show that for all cases tested, the steady current obtained by using the analytical model is always inside the confidence interval of the experimental data from the bottom to the canopy top. Below the top of the canopy the steady current is around 10% the horizontal wave orbital velocity. At the top of the canopy the steady current goes shoreward. This behaviour was already reported experimentally and numerically by Luhar et al. (2013, 2010); van Rooijen et al. (2020); Abdolahpour et al. (2017). Additionally, the skimming flow at the top of the canopy is well reproduced, and the current inside the canopy is basically depth-uniform. From the top of the canopy to the free surface, a seaward current is observed. This seaward current is identified by the model in agreement with van Rooijen et al. (2020); Luhar et al. (2010). Nonetheless, for $R1$ and $R2$ the analytical model presents the largest deviation with respect to the experimental data. Two possible sources of error are attributed to these discrepancies: 1) the wave height decay formulation used in the present model assumes a

linear wave theory, so the pressure gradient is being underestimated; and 2) the last term on the right hand side of Eq.(29) is a linear function dependent of the water depth and proportional to U_c. In addition, the seaward current above the top of the canopy is depth-dependent and follows a parabolic profile as demonstrated in Eq.(29). Finally, the lower the KC number (KC in Table 1) the least the effect by the pressure gradient on the seaward current in the analytical model (as observed in Figure 1).

3.2 Flexible canopy

To test the analytical model for the steady current induced in flexible canopies, the canopy frontal area has been modified by an stem-effective length to account for the biased position induced by the streaming. Following Luhar et al. (2013, 2017) this length is function of the Cauchy (Ca) and Buoyancy (B) numbers. In addition, for the RANS model velocity, possible departures from the steady current due to turbulent fluctuations or systematic errors are not possible to be assessed by confidence intervals.

The normalized wave induced steady currents in flexible canopies are shown in Figure 2 showing a good performance at the top of the canopy (the shoreward current) for both wave conditions. Above the canopy, the seaward current from the analytical formulation and RANS model are in agreement for $CM1$, but not for $CM2$ where the analytical model presents a lower value. For flexible canopy scenarios it seems that the wave non-linearity influences the seaward current estimation. The higher the Ur the bigger the difference between the RANS and the analytical model. So, the pressure gradient is being underestimated for non-linear wave conditions.

3.3 General discussions

Concerning the steady current at mid-canopy, the profile can be split in three regions (see Figure 3). $Z1$, above the canopy top, shows a parabolic seaward current as the result of the balance between pressure gradient and mass conservation restriction (the linear function on the last term of the right hand side of equation (29)). $Z2$, at the canopy top, presents a skimming flow shoreward where the pressure gradient, the wave stress, steady current-wave drag force, and mass conservation restriction are involved. $Z3$, below the canopy top, presents a very low velocity magnitude where the momentum balance is between the pressure gradient, the steady current-wave interaction drag force, and mass conservation restriction. Below the top of the canopy, the steady current given by the analytical model predicts a shoreward current while the RANS simulations and experimental data show a seaward current, but, $\overline{u}$ is less than 10% $U_{\infty,rms}$ for all scenarios. Nonetheless, ADV experimental data in Abdolahpour et al. (2017) and Particle Image Velocimetry data in van Veelen et al. (2020) reported some shoreward currents scenarios.

Finally, Figure 1 and Figure 2 show an analytical solution neglecting the pressure gradient term where is possible to observed how this term contributes to the seaward current above the canopy top and intensifies the skimming flow at the top of the canopy (scenarios where the pressure gradient is included). In addition, the steady current over a flat bottom and no canopy (upstream the canopy) (see Figure 3) presents a similar behavior to a mean flow in Longuet-Higgins (1953), where a wave height decay is produced by the viscous dissipation when the wave interacts with the bottom (Luhar et al., 2010). In this region, the first term (pressure gradient) and the last term on the right hand side of equation (29) define the steady current profile. This result is in agreement with the experimental work in Luhar et al. (2010); Abdolahpour et al. (2017).

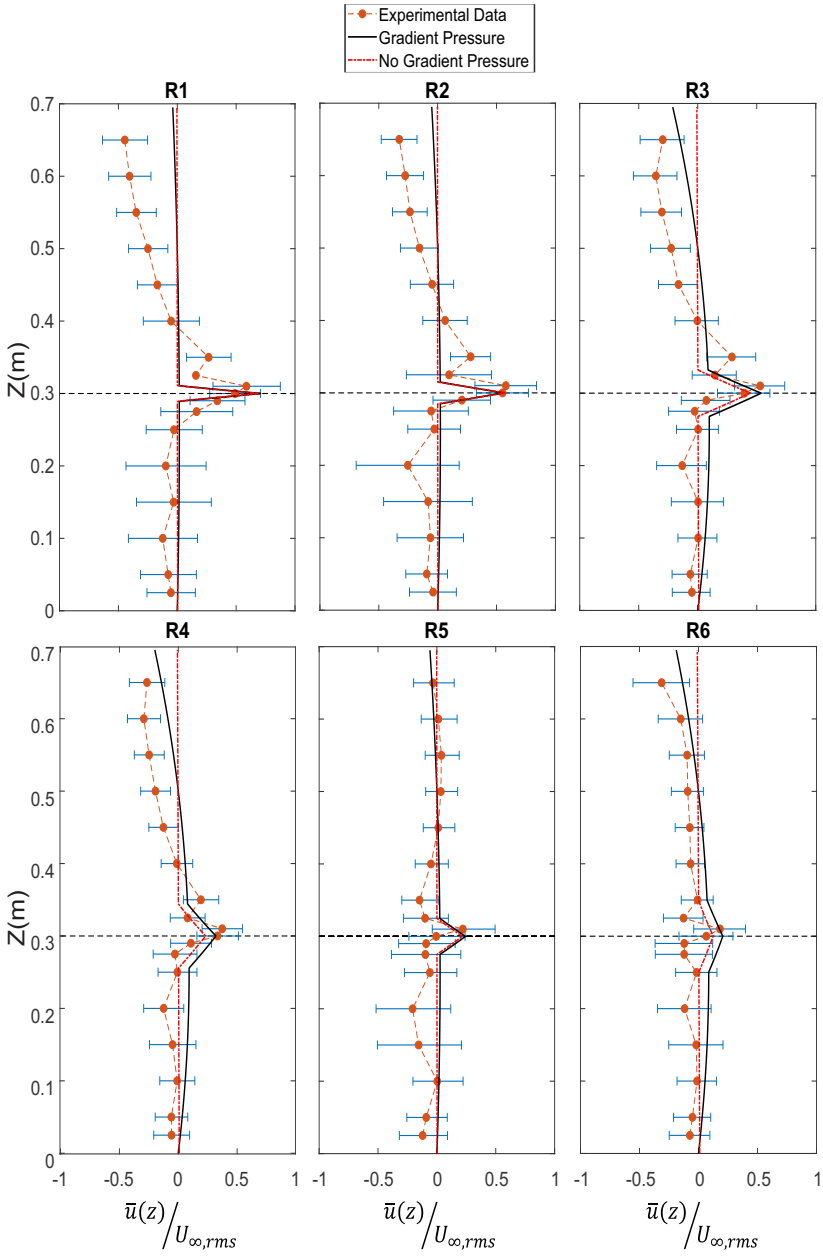

Figure 1. Normalized wave-induced steady current, $\overline{u(z)}$. $U_{\infty,rms}$ is the horizontal root mean square wave orbital velocity far from canopy effects. Orange dot-dashed line is the experimental data, blue line the confidence interval. The continuous black and red dashed lines are the analytical model including the pressure gradients and neglecting the pressure gradient, respectively. The horizontal dashed line indicates the canopy top.

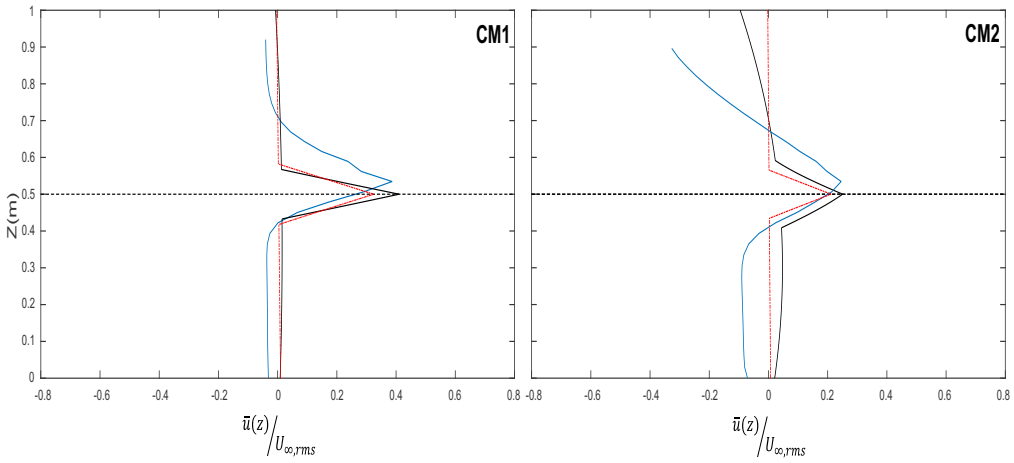

Figure 2. Normalized wave-induced steady current. $U_{\infty,rms}$ is the horizontal wave orbital velocity far from canopy effects. The blue corresponds to the $RANS - VOF$ model by Maza et al. (2013), and the continuous black and red dashed lines are the analytical model with and without the pressure gradient, respectively.

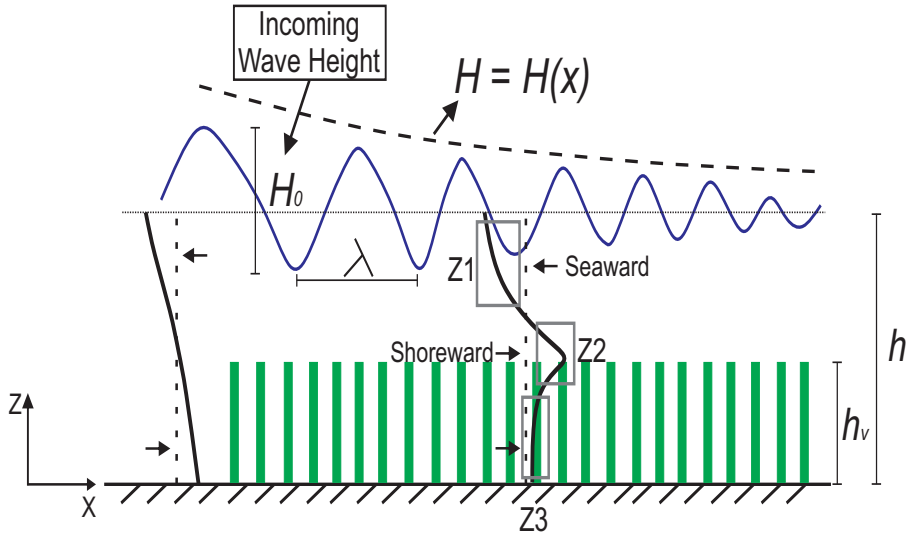

Figure 3. Qualitative scheme for the wave-induced steady current. Dashed line represents the vertical axis of the velocity profile. Upstream is the steady current profile with no canopy. Mid-canopy represents the steady current vertical profile under aquatic vegetation-wave interaction.

4 Conclusions

In this work we provide a step forward to a better understanding of the mechanisms involved in the wave-induced steady current under wave-canopy interaction by formulating a simple analytical model. The development is performed by a dimensional analysis to the momentum equation satisfying the mass conservation. The model, expressed by a polynomial function, can be easily implemented in large scale phase averaged coastal models in order to include the wave-induced steady current created by aquatic canopies-wave interaction.

The development of the analytical model revealed the dominant terms driving the wave-induced steady current. Some of the terms discussed in this work were introduced in previous studies by using numerical simulations, however, this is the first approach from analytical departure solving a depth-dependent wave-induced steady current. Additionally, the influence by the wave decay (pressure gradient) on inducing the seaward current above the canopy and its contribution to the skimming flow at the top of the canopy was also revealed in this work.

The highest discrepancies between the analytical model and experimental/RANS data are observed above the canopy top, the seaward direction. These differences are attributable to the underestimation in the pressure gradient since we assumed a linear wave decay. Thus, the development of wave decay statements based on nonlinear wave theory is further needed.

The wave-induced steady current can be split in three regions. Above the canopy top (a balance between the mass conservation restriction and pressure gradient) a seaward current is observed. At the top of the canopy a shoreward current is realised and intensified when including the pressure gradient term. Inside the canopy where the steady flow is weak compared with the other two regions. Additionally, in the present study a parametrization to the wave stress term is defined, however, investigations to the wave stress gradient term is needed in order to improve the steady current calculations.

Acknowledgments

A. Cáceres-Euse thanks SINAPSI project (ICAR/02 COSTRUZIONI IDRAULICHE E MARITTIME E IDROLOGIA) for postdoctoral fellowship support. A. Orfila acknowledged financial support from the Spanish Government MICINN/FEDER through MOCCA Project (RTI2018-093941-B-C31). M. Maza, is sincerely grateful to the Spanish Ministry of Science, Innovation and Universities for the funding provided in the grant Juan de la Cierva Incorporation (BOE de 27/10/2017) and for the financial support through SHACC project (RTI2018-097014-B-I00). Authors thank Arnold Van Rooijen for providing the experimental data used in this work (van Rooijen et al., 2020).

5 Appendix

The parameters used to calculate the wave-induced steady currents are defined as follows,

$$C_d = 0.87 + \left(\frac{2200}{Re_d}\right)^{0.88}, \qquad Re_d = \frac{a_v U_\infty}{\nu}$$

$$f_w = exp\left[5.123\left(\frac{K_b}{A_w}\right)^{0.1944} - 5.977\right]$$

$$\xi = \frac{2ka_vC_d}{9\pi}\left[\frac{9sinh(kh_v)+sinh(3kh_v)}{sinh(kh)(sinh(2kh)+2kh)}\right]$$

where K_b is the hydraulic roughness and given that the inertial term in the canopy resistance is negligible ϕ can be defined based on Lowe et al. (2005),

$$\phi = \sqrt{\frac{C_f(1-\lambda_p)}{C_d\lambda_f}}$$

where the empirical friction coefficient is assumed $C_f \sim 0.01$, however, future improvements to the model can include a parametrization as function of the flow condition.

To solved the Reynolds stress in Equation (29) a formulation based on Prantdl mixing-length hypothesis in Cáceres-Euse et al. (2021) has been used,

$$\overline{u'w'} = -\nu_t\frac{\partial\overline{u}}{\partial z} \Rightarrow u_*^2 \sim \nu_t\frac{U_{\infty,rms}}{\delta}$$

and assuming $u_* \sim 0.1U_{\infty,rms}$ (Lowe et al., 2005),

$$\nu_t \sim \frac{\delta U_\infty^{rms}}{100}$$

For simplicity, ν_t has been assumed constant and dependent on the wave properties and canopy drag.

References

Abdolahpour, M., Ghisalberti, M., Lavery, P., & Mcmahon, K. (2016). Vertical mixing in coastal canopies. *Limnology and Oceanography*, *62*, 26-42. doi: 10.1002/lno.10368

Abdolahpour, M., Ghisalberti, M., McMahon, K., & Lavery, P. S. (2020). Material Residence Time in Marine Canopies Under Wave-Driven Flows. *Frontiers in Marine Science*, *7*, 1-11. doi: 10.3389/fmars.2020.00574

Abdolahpour, M., Hambleton, M., & Ghisalberti, M. (2017). The wave-driven current in coastal canopies. *Journal of Geophysical Research: Oceans*, *122*, 3660-3674. doi: 10.1002/2016JC012446

Bricker, J. D., & Monismith, S. G. (2007). Spectral wave-turbulence decomposition. *Journal of Atmospheric and Oceanic Technology*, *24*, 1479-1487. doi: 10.1175/JTECH2066.1

Cáceres-Euse, A., Orfila, A., Maryam, A., Toro-Botero, F., Variano, E. A., & Osorio, A. (2021). Analytical solution for the Kelvin–Helmholtz instability under a submerged canopy-oscillatory flow. *Journal of Hydraulic Research*, 1-9. doi: 10.1080/00221686.2021.190843

Cáceres-Euse, A., Variano, E. A., Toro-Botero, F., Gómez-Giraldo, A., & Osorio, A. (2020). Simplified approach to oscillatory flow-submerged canopy. *Journal of Hydraulic Engineering*, *146*, 1-13. doi: 10.1061/(ASCE)HY.1943-7900.0001807

Chen, H., Liu, X., & Zou, Q. P. (2019). Wave-driven flow induced by suspended and submerged canopies. *Advances in Water Resources*, *123*, 160-172. doi: 10.1016/j.advwatres.2018.11.009

Dalrymple, R. A., Kirby, J. T., & Hwang, P. A. (1984). Wave Diffraction Due To Areas of Energy-Dissipation. *Journal of Waterway Port Coastal and Ocean Engineering-ASCE*, *110*, 67–79.

Duarte, C. M., Marbá, N., Gacia, E., Fourqurean, J. W., Beggins, J., Barrón, C., & Apostolaki, E. T. (2010). Seagrass community metabolism: Assessing the carbon sink capacityof seagrass meadows. *Global Biogeochemical Cycles*, 1-8. doi: 10.1029/2010GB003793

Etminan, V., Lowe, R. J., & Ghisalberti, M. (2019). Canopy resistance on oscillatory flows. *Coastal Engineering*. doi: 10.1016/j.coastaleng.2019.04.014

Finnigan, J. (2000). Turbulence in Plant Canopies. *Annual Review of Fluid Mechanics*, *32*, 519-571.

Foster-Martinez, M. R., Lacy, J. R., Ferner, M. C., & Variano, E. A. (2018). Wave attenuation across a tidal marsh in San Francisco Bay. *Coastal Engineering*, *137*, 26-40. doi: https://doi.org/10.1016/j.coastaleng.2018.02.001

Ghisalberti, M., & Nepf, H. M. (2002). Mixing layers and coherent structures in vegetated aquatic flows. *Journal Of Geophysical Research*, *107*, 1-11. doi: 10.1029/2001JC000871

Ghisalberti, M., & Schlosser, T. (2013). Vortex generation in oscillatory canopy flow. *Journal of Geophysical Research: Oceans*, *118*, 1534-1542. doi: 10.1002/jgrc.20073

Infantes, E., Orfila, A., Simarro, G., Terrados, J., Luhar, M., & Nepf, H. (2012). Effect of a seagrass (Posidonia oceanica) meadow on wave propagation. *Marine Ecology Progress Series*, *456*, 63-72. doi: 10.3354/meps09754

Jacobsen, N. G. (2016). Wave-averaged properties in a submerged canopy: Energy density, energy flux, radiation stresses and Stokes drift. *Coastal Engineering*, *117*, 57-69. doi: 10.1016/j.coastaleng.2016.07.009

Jensen, B. L., Sumer, B. M., & Fredsoe, J. (1989). Turbulent oscillatory boundary layers at high Reynolds numbers. *Journal of Fluid Mechanics*, *206*, 265-297.

Kobayashi, N., Raichle, A. W., & Asano, T. (1993). Wave Attenuation by Vegetation. *Journal of Waterway, Port, Coastal, and Ocean Engineering*, *119*, 30-48.

Lei, J., & Nepf, H. (2019). Wave damping by flexible vegetation: Connecting individual blade dynamics to the meadow scale. *Coastal Engineering*, *147*, 138-148. doi: 10.1016/j.coastaleng.2019.01.008

Longuet-Higgins, M. (1953). Mass transport in water waves. *Philos. Trans. R. Soc. London A*, *245*, 535–581.

Losada, I. J., Maza, M., & Lara, J. L. (2016). A new formulation for vegetation-induced damping under combined waves and currents. *Coastal Engineering*, *107*, 1-13. doi: 10.1016/j.coastaleng.2015.09.011

Lowe, R., Koseff, J., & Stephen, M. (2005). Oscillatory flow through submerged canopies: 1. Velocity structure. *Journal of Geophysical Research*, *110*, C10016. doi: 10.1029/2004JC002788

Luhar, M., Coutu, S., Infantes, E., Fox, S., & Nepf, H. M. (2010). Wave induced velocities inside a model seagrass bed. *Journal of Geophysical Research*, *115*, C12005. doi: 10.1029/2010JC006345

Luhar, M., Infantes, E., & Nepf, H. (2017). Seagrass blade motion under waves and its impact on wave decay. *Journal of Geophysical Research: Oceans*. doi: 10.1002/2016JC012264.Received

Luhar, M., Infantes, E., Orfila, A., Terrados, J., & Nepf, H. M. (2013). Field observations of wave-induced streaming through a submerged seagrass (Posidonia oceanica) meadow. *Journal of Geophysical Research: Oceans*. doi: 10.1002/jgrc.2

Maxwell, P. S., Eklöf, J. S., van Katwijk, M. M., O'Brien, K. R., de la Torre-Castro, M., Boström, C., ... van der Heide, T. (2017). The fundamental role of ecological feedback mechanisms for the adaptive management of seagrass ecosystems – a review. *Biological Reviews*, *92*, 1521-1538. doi: 10.1111/brv.12294

Maza, M., Lara, J. L., & Losada, I. J. (2013). A coupled model of submerged vegetation under oscillatory flow using Navier-Stokes equations. *Coastal Engineering*, *80*, 16-34. doi: 10.1016/j.coastaleng.2013.04.009

Mazda, Y., Wolanski, E., King, B., King, B., Akira, S., Daisuke, O., & Michimasa, M. (1997). Drag force due to vegetation in mangrove swamps. *Mangroves and Salt Marshes*, *1*, 193–199. doi: 10.1023/A:1009949411068

Nepf, H. M. (2012). Flow and Transport in Regions with Aquatic Vegetation. *Annual Review of Fluid Mechanics*. doi: 10.1146/annurev-fluid-120710-101048

Nielsen, P. (1992). *Coastal bottom boundary layers and sediment transport. world scientific publishing co inc.*

Rodi, W. (1993). *Turbulence Models and Their Applications in Hydraulics: A State of the Art Review.*

Tanino, Y., & Nepf, H. (2008). Laboratory Investigation of Mean Drag in a Random Array of Rigid, Emergent Cylinders. *Journal of Hydraulic Engineering*. doi: 10.1061/(ASCE)0733-9429(2008)134:1(34)

van Rooijen, A., Lowe, R., Rijnsdorp, D. P., Ghisalberti, M., Jacobsen, N. G., & McCall, R. (2020). Wave-Driven Mean Flow Dynamics in Submerged Canopies. *Journal of Geophysical Research: Oceans*, *125*. doi: 10.1029/2019JC015935

van Veelen, T., Fairchild, T. P., Reeve, D., & Karunarathna, H. (2020). Experimental study on vegetation flexibility as control parameter for wave damping and velocity structure. *Coastal Engineering*, *157*. doi: doi.org/10.1016/j.coastaleng.2020.103648

Zhang, Y., Tang, C., & Nepf, H. (2018). Turbulent Kinetic Energy in Submerged Model Canopies Under Oscillatory Flow. *Water Resources Research*, *54*, 1734-1750. doi: 10.1002/2017WR021732